ARTICLE

Developing design criteria for organic solar cells using well-absorbing non-fullerene acceptors

Lisa Krückemeier [1,2], Pascal Kaienburg [1], Jan Flohre[1], Karsten Bittkau [1], Irene Zonno [1], Benedikt Krogmeier [1] & Thomas Kirchartz [1,2]

In recent years, efficiencies of bulk heterojunction solar cells have risen substantially mostly due to the development of well-absorbing small molecules that replace fullerenes as the acceptor molecule. The improved light absorption due to the combination of two strongly absorbing molecules raises the question, how to best combine the absorption onsets of the donor and acceptor molecule to maximize efficiency. By using numerical simulations, we explain under which circumstances complementary absorption or overlapping absorption bands of the two molecules will be more beneficial for efficiency. Only when mobility and lifetime of charge carriers are sufficiently high to allow sufficient charge collection for layer thicknesses around the second interference maximum, a combination of complementary absorbing molecules is more efficient. For smaller thicknesses, a blend of molecules with the same absorption onset achieves higher efficiencies.

[1] IEK5-Photovoltaics, Forschungszentrum Jülich, 52425 Jülich, Germany. [2] Faculty of Engineering and CENIDE, University of Duisburg-Essen, Carl-Benz-Strasse 199, 47057 Duisburg, Germany. Correspondence and requests for materials should be addressed to L.Küc. (email: l.krueckemeier@fz-juelich.de) or to T.K. (email: t.kirchartz@fz-juelich.de)

High absorption coefficients of organic molecules make them attractive for photovoltaic applications[1]. However, the high absorption coefficients come with the downside of exciton binding energies that are much higher than in inorganic materials. Splitting the exciton therefore requires a type II heterojunction between an electron-donating and an electron-accepting molecule. While the process of exciton dissociation and charge generation in organic solar cells has frequently worked remarkably well[2–6] in the past, this was often—at least partly—due to the acceptor molecule being a fullerene. However, the predominance of fullerenes has been an obstacle for high performance. While fullerenes do absorb light and may contribute substantially to the photocurrent[7], they do not absorb light as efficiently as the typically used donor molecules[8]. Thus, the percentage of fullerene molecules in the film had to be limited for reasons of high absorption even if a higher fullerene concentration would have been helpful for better charge transport[9,10]. Till recently, photovoltaic devices using non-fullerene-based acceptor molecules (NFAs) have not shown high performances[11,12]. This has changed in the last few years and a variety of new non-fullerene acceptor molecules are now available and often achieve higher efficiencies than their fullerene-based counterparts[13–21]. This is due to non-fullerene acceptors absorbing light more efficiently[15] and due to open-circuit voltage losses being reduced relative to the case of devices based on fullerene acceptors[18,21–24]. The variety of available non-fullerene acceptors also provides great flexibility in the choice of energy gaps and positions of the HOMO (highest occupied molecular orbital) and LUMO (lowest unoccupied molecular orbital) levels. This high flexibility does not exist when using fullerenes, which mainly absorb in the ultraviolet (UV) range of the spectrum and whose energy levels are typically changed by using fullerene multiadducts which rarely show good photovoltaic performance[25].

When trying to optimize the absorption spectra and energy levels of donor and acceptor molecules, different design criteria apply[26] to the situation of donor molecules combined with less strongly absorbing fullerenes or with highly absorbing small-molecule acceptors. With two molecules contributing roughly equally to the total absorptance, the question arises what the ideal band gaps or absorption onsets for the molecules should be. The answer to this question is affected by a series of parameters such as the voltage loss between absorption onset and open-circuit voltage, the spectral width of the absorption of the molecules and the product of peak absorption coefficient and layer thickness.

The aim of this article is to develop design criteria for when to choose either complementary or congruent (overlapping) absorption spectra of donor and acceptor molecules. By taking these design criteria into account, the new flexibility and the promising absorption properties of the NFAs can be utilized and thus contribute to an optimization of the solar cell performance. To develop these criteria, we investigate and systematically differentiate the influence of the various parameters mentioned above.

Results

Model. First, we take a closer look at the absorption spectra of organic semiconductors and formulate a suitable parameterization of the absorption coefficient $\alpha(E)$. The parameterization of $\alpha(E)$ should reflect the important features of the experimental behavior. In addition, this parameterization provides a basis for the further determination of the absorption coefficient $\alpha_{eff}(E)$ of the donor–acceptor blend, as well as the absorptance $a(E)$ of the active layer and finally the solar cell efficiency η_{eff}.

Unlike in the case of inorganic semiconductors, organic semiconductors have a high absorption coefficient only in a limited spectral region with a typical width of about ~0.5 eV[1]. As an example, Fig. 1a shows the measured absorption coefficients of the non-fullerene acceptors FBR[27] and IDTBR[28], the donor polymer PTB7-Th[29,30], and their blends (Supplementary Fig. 1 shows the molecular structures). A particular feature being typical for organic semiconductors is that the shape of the absorption peak is asymmetric with the rising edge at lower energies being steeper than the decay at higher energies[1].

We simulate this absorption behavior by using a parameterization, in which the absorption coefficient of the organic material is formed by the product of two distribution functions (error functions). This approach allows us to have parameters to adjust the absolute height of the absorption coefficient (α_0), the width of the rising and falling edge (σ_{up}, σ_{down}), and the distance (ΔE) between the inflection points of rising and falling edge. The curves of the absorption coefficients $\alpha_1(E)$ and $\alpha_2(E)$ illustrated in Fig. 1b are examples of this parameterization. In order to have a consistent definition for the absorption edge, we choose the inflection points of the absorption coefficient as the characteristic energy of the absorption onset or band gap of the material[31]. The supplementary information (Eqs. S1–S5, Supplementary Table 1, and Supplementary Figs. 2 and 3) provides a detailed overview of the used equations and parameters whose variation adjusts the peak shape and height.
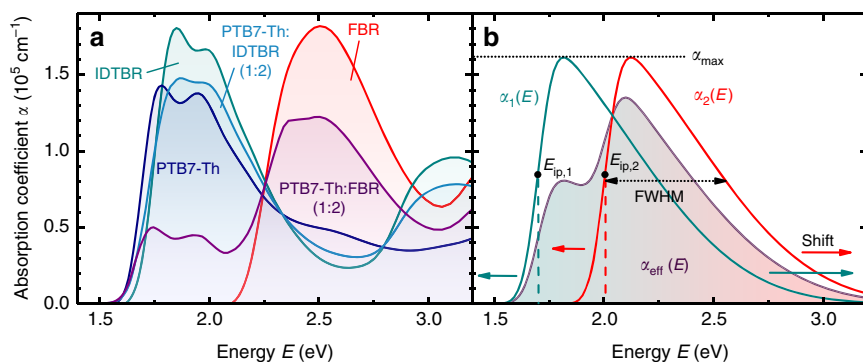

Fig. 1 Comparison between the experimental and simulated absorption coefficients of organic molecules for OPV. (**a**) Absorption coefficients of the non-fullerene acceptors FBR[27] (red) and IDTBR[28] (cyan), the donor polymer PTB7-Th[29,30] (blue), and their blends (ratio 1:2) (light blue, purple) determined from UV–Vis measurements. (**b**) Exemplary curves of simulated absorption coefficients $\alpha_1(E)$ and $\alpha_2(E)$ representing the organic donor and acceptor material. The coefficient α_{max} and the full-width half-max (FWHM) describe the strength and shape of the absorption peak. In addition, the energies $E_{ip,1}$ and $E_{ip,2}$ indicate the inflection points of the corresponding absorption edges whose variation causes a shift in peak position. The effective absorption coefficient $\alpha_{eff}(E)$ of the blend material, used in our simulations, results from the superposition of the respective absorption coefficients $\alpha_1(E)$ and $\alpha_2(E)$. The corresponding parameters of the simulation are listed in Supplementary Table 1, and $E_{ip,1} = 1.7$ eV and $E_{ip,2} = 2$ eV

Contrary to the traditional assumption that a significant energy offset between the donor and acceptor levels is necessary to provide a driving force for exciton dissociation[25,32,33], recent developments in material science for organic photovoltaics (OPVs) have shown that some non-fullerene organic solar cells (OSCs) with type II heterojunctions exhibit fast and efficient charge separation despite having a negligible energy offset[18,34]. In these cases, no spectral signature is observed in absorption or luminescence spectra that can be directly attributed to the charge-transfer state, suggesting that the energy E_{CT} of the charge-transfer state is very close to that of either the donor or acceptor molecule. For the purpose of this article, we therefore choose this best-case scenario, where the luminescence of the donor–acceptor blend is not red-shifted relative to the emission of either donor or acceptor. Thus, the effective absorption coefficient $\alpha_{eff}(E)$ of the blend results from the superposition of the donor and acceptor behavior described by the coefficients $\alpha_1(E)$ and $\alpha_2(E)$. As a further simplification, we also assume that the absorption coefficients of the donor and acceptor materials, which have the same peak shape but differ in their spectral position, contribute equally to the total absorption of the blend. A shift of the energetic position, adjustable by varying the respective inflection-point energy E_{ip}, leads to different effective absorption coefficients $\alpha_{eff}(E)$. In this way, different absorption characteristics of the blend material can be produced, ranging from congruent ($E_{ip,1} = E_{ip,2}$) to complementary ($E_{ip,2} \gg E_{ip,1}$). These effective absorption spectra differ in their spectral distribution, shape, and height, as well as their position of the absorption onset. The purple spectrum in Fig. 1b is an example of an effective absorption coefficient $\alpha_{eff}(E)$ generated in this way. It results from a superposition of the single spectra $\alpha_1(E)$ and $\alpha_2(E)$ also presented in Fig. 1b as red and cyan lines.

A systematic energy shift of the two absorption peaks is used to answer the initial question, how the absorption onsets of the two organic materials should be arranged in order to achieve the highest possible efficiency η_{max}. These simulations enable us to develop design criteria for organic solar cells with well-absorbing non-fullerene acceptors, in which donor and acceptor contribute equally to absorption.

Note that determining the efficiency η requires us to calculate the absorptance $a_{eff}(E)$ of the photoactive layer from the effective absorption coefficient, the absorber layer thickness d, and an optical model. In the first part of the paper, we intend to keep the discussion generic (and not layer-stack specific) so we use a simple Lambert–Beer-type model without interferences. In the last section ("Simulations with optical interferences and collection losses"), we assume a specific layer stack which allows us to include interferences in our optical model. The simple Lambert–Beer model for the absorptance used in the first part of the paper assumes complete reflection at the rear contact of the solar cell and neglects reflection at the front or parasitic absorption. Thereby, the absorptance $a_{eff}(E)$ increases monotonously with increasing layer thickness d of the absorber and is given by

$$a_{eff}(E) = 1 - \exp(-2\alpha_{eff}(E)d). \quad (1)$$

In addition, we assume in the first part of the paper that charge collection is efficient, that is, that the external quantum efficiency $Q_e(E)$ is equal to the absorptance. Thus, we calculate the short-circuit current J_{sc} density via

$$J_{sc} = q \int_0^\infty a_{eff}(E)\phi_{sun}(E)dE, \quad (2)$$

where q is the elementary charge and $\phi_{sun}(E)$ is the AM 1.5G solar spectrum. The optimum J_{sc} therefore only depends on the

product $\alpha_{eff}(E)d$, which is however an energy-dependent quantity. For a given shape ($\alpha_0 = 2.2 \times 10^5\,cm^{-1}$, $\sigma_{up} = 0.08\,eV$, $\sigma_{down} = 0.6\,eV$, $\Delta E = 0.4\,eV$) the absorption coefficient is entirely characterized by its maximum value. Thus, we use the product $\alpha_{max}d$ in the following as one of the key parameters controlling the value of the optimum inflection points $E_{ip,1}$ and $E_{ip,2}$.

In order to be able to perform the calculation of the efficiency η, an expression for the open-circuit voltage V_{oc} is required. Non-radiative recombination losses are a significant loss mechanism in organic solar cells reducing the achievable open-circuit voltage V_{oc} and thereby the efficiency η. The mechanisms causing these losses and being responsible for their high extent in organic solar cells are not fully understood yet. A common and frequently used approach is Langevin's theory of bimolecular and diffusion-limited recombination[35], which however often fails to provide an accurate description of experimental behavior[36–38]. Langevin recombination assumes losses independent of the energy gap between the excited and the ground state. However, according to Benduhn et al.[39], there is an empirical relation between the non-radiative recombination rate and the energy gap between the excited charge-transfer and the ground state. This relation results if we assume that the diffusion of carriers towards each other (and the donor–acceptor interface) is not the slowest step in recombination. Instead, we have to assume that the dissipation of energy by excitation of molecular vibrations limits the time constant of non-radiative recombination. The non-radiative recombination rate shows an approximately exponential dependence on the energy gap in semiconductors[40,41], large organic molecules[42], and complexes[43]. This loss mechanism would then be intrinsic, caused by molecular vibrations of the C–C bonds in organic semiconductors[39].

The magnitude of non-radiative voltage losses ΔV_{nr} depends on the internal reorganization energy λ and the energy E_{CT} of the charge-transfer state, which is the energy difference between the ground state and the CT excited state. In addition, it may also depend on the molecular packing and the alignment of donor and acceptor molecules at the donor–acceptor interface[44,45]. Increasing this charge-transfer state energy reduces non-radiative losses, because these transitions become less likely for larger energy gaps, since more phonons are involved. The non-radiative recombination rate k_{nr} is approximately proportional to the so-called Franck–Condon factor $S^p e^{-S}/p!$ and is thereby linked to the number p of vibrational modes necessary for the transition[46,47]. This number, in turn, is given by $E_{CT}/\hbar\omega$, where $\hbar\omega$ is the mean energy of a phonon involved in the transition. S is the so-called Huang–Rhys factor, which is associated with the strength of the electron–phonon coupling and which is in the order of 1 in organic semiconductors[48,49]. The Franck–Condon factor has the mathematical form of a Poisson distribution and has a peak at $S = p$ and decays strongly for the practically relevant case where $p \gg S$ (typical values of p are on the order 10). The dependence of k_{nr} on E_{CT} translates into a dependence of the non-radiative voltage loss ΔV_{nr} on E_{CT}. For this article, we use the empirical relation

$$\Delta V_{nr} = 0.547\,V - 0.184\,VeV^{-1}(E_{CT} - \lambda) \quad (3)$$

introduced in ref.[39] to account for energy-gap-dependent non-radiative voltage losses.

The energy E_{CT} of the charge-transfer state corresponds to the energy at the intersection between normalized absorptance $a_{eff}(E)$ and normalized electroluminescence $\phi_{EL}(E)$ of the blend material[50]. Fig. 2 shows an example of this definition for both Fig. 2a experimentally determined and Fig. 2b simulated spectra. For a red-shifted absorptance and EL emission, also a smaller energy for the charge-transfer state is obtained. Hence, in a blend material consisting of two organic semiconductors, the one with
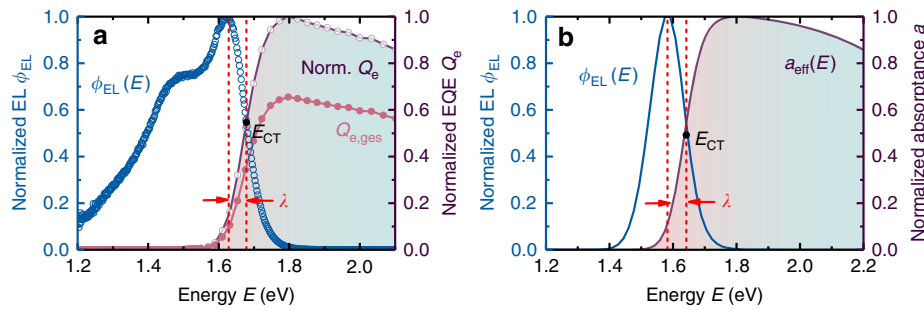
Fig. 2 Definition of the charge-transfer state energy E_{CT} and the internal reorganization energy λ. Comparison of (**a**) experimental and (**b**) simulated normalized electroluminescence spectra $\phi_{EL}(E)$ and the external quantum efficiency $Q_e(E)$ and absorptance $a_{eff}(E)$, respectively. The energy at the intersection point of the normalized absorptance $a_{eff}(E)$ and the EL emission $\phi_{EL}(E)$ of the blend material defines the energy E_{CT} of charge-transfer state, which is used to calculate the non-radiative voltage losses according to ref[39]. In addition, the internal reorganization energy λ, defined by the distance between charge-transfer state energy E_{CT} and the maximum of the EL spectrum, is also incorporated into the calculation of the non-radiative losses ΔV_{nr}. A broadening of the absorption onset further results in a red shift of the EL spectrum, as a result of an increasing energy λ. A red shift of absorptance and EL emission is accompanied by a lower charge-transfer energy E_{CT}, leading to higher non-radiative voltage losses

the smaller energy gap decisively determines the amount of non-radiative losses. Furthermore, the internal reorganization energy λ affects the amount of non-radiative losses. As shown in Fig. 2, the distance between the charge-transfer state energy E_{CT} and the maximum of the EL spectrum defines the value of reorganization energy λ, which increases for example with a spectral broadening of the absorption onset.

If the recombination losses, the absorption coefficient of the blend, and an optical model are defined, we are able to calculate the open-circuit voltage via[51,52]

$$V_{oc} = \frac{k_B T}{q} \ln\left(\frac{J_{sc}}{J_{0,rad}}\right) - \Delta V_{nr} \text{ for } J_{sc} \gg J_{0,rad} \quad (4)$$

with the Boltzmann constant k_B, the temperature T, the saturation-current density

$$J_{0,rad} = q \int_0^\infty a_{eff}(E)\phi_{bb,300K}(E)\,dE \quad (5)$$

in the radiative limit, the short-circuit current density J_{sc} according to Eq. (2), and $\phi_{bb,300K}(E)$ the black body spectrum at 300 K. The external light-emitting diode (LED) quantum efficiency Q_{LED} is linked to the non-radiative voltage losses by[52,53]

$$Q_{LED} = \exp\left(-\frac{q\Delta V_{nr}}{k_B T}\right). \quad (6)$$

The current–voltage characteristic of the solar cell is then given by

$$J = \frac{J_{0,rad}}{Q_{LED}} \cdot \left(\exp\left(\frac{qV}{k_B T}\right) - 1\right) - J_{sc}. \quad (7)$$

The electrical power density $P = -JV$ results from the multiplication of total current density J and voltage V. Finally, the efficiency η of the solar cell is calculated by weighting the maximum electrical power density with the incident power density P_{sun} of the sun according to the AM 1.5G spectrum, so η = max$(P)/P_{sun}$. In the ideal case—which neglects the series resistance from the contacts and assumes an ideal diode—the fill factor (FF) only depends on V_{oc}[54] and has values around 90%. We use this ideal FF behavior[54] in the first two parts of the paper (subsections "Simulations with ideal collection and absorption properties," "Simulations with parameterized absorption coefficients") and thus assume ideal transport properties where all generated charge carriers can be collected. For real n–i–p-type

thin film solar cells, the FF strongly depends on the thickness d of the active layer and the electrical transport properties of the absorber materials itself[55–59]. Therefore, in the subsequent simulations in the last part of this paper ("Simulations with optical interferences and collection losses"), electronic losses in the active layer are included. For organic solar cells with NFA-based blends, the FF is often between 60 and 75%[15,18,19,60–63] even for devices with thin active layers of about 100 nm, while certain fullerene-containing blends exceed 70% FF at thicknesses above 200 nm[64–67]. High FFs are enabled by efficient charge carrier collection which is governed by the ratio between how long charge carriers are free before they recombine versus how long it takes them to reach the contacts where they are extracted[57–59]. Therefore, the thickness of the blend layer does not only influence its absorptance a_{eff} but also the FF[55], because it determines the average distance that charge carriers need to travel before being extracted at the contacts. Previously[55], we have expressed the competition between transport and recombination by the electronic quality factor

$$Q = \frac{\mu^2}{k^{0.8}}, \quad (8)$$

where μ is the mobility and k is the coefficient of direct recombination. For undoped devices, the FF is affected by thickness and built-in voltage, which are independent of the absorber material, and the photo-generation rate of charge carriers. After eliminating the influence of these parameters on the FF, the FF only depends on the electronic quality factor Q which is a material-specific quantity. As a consequence, the choice of a certain donor–acceptor combination will not only determine the spectral shape of absorption but also affect the blend's Q—and therefore the FF of the resulting solar cell.

To reach a realistic description for typical organic solar cell devices in the subsection "Simulations with optical interferences and collection losses," we will—in addition to considering charge-collection issues—drop the simple Lambert–Beer model for absorption expressed in Eq. (1) by taking interference into account which introduces absorptance maxima at certain thicknesses. We optically simulate a typical n–i–p cell stack composed of glass/ITO (150 nm)/ZnO (40 nm)/PTB7-Th:NFA (1:2)/MoO$_3$ (10 nm)/Ag (100 nm). The thickness d of the active layer is varied. Optical simulations are based on the Transfer Matrix Method[68]. The resulting generation profiles under AM 1.5G illumination are used as input to numerical drift-diffusion simulations of the charge carrier dynamics with the Advanced

Semiconductor Analysis (ASA) software (https://www.tudelft.nl/en/eemcs/the-faculty/departments/electrical-sustainable-energy/photovoltaic-materials-and-devices/software-platform/asa-software/), which generates current–voltage data. The electronic simulation parameters are listed in Supplementary Table 2.

Our main goal in the subsection "Simulations with optical interferences and collection losses" is to illustrate, for a given absorption spectrum, the influence of interference and electronic quality on the thickness dependence of the efficiency. We compare the two cases of congruent and complementary
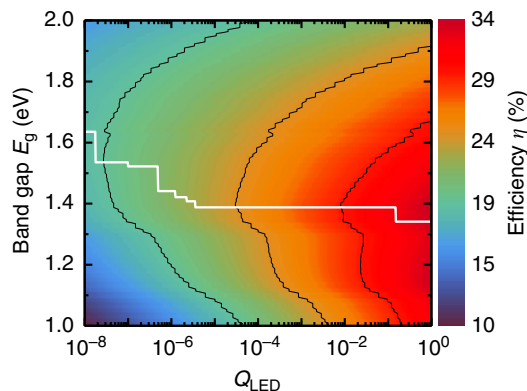

Fig. 3 Simulation with ideal collection and absorption properties. Contour plot of the efficiency η of a solar cell with ideal collection properties and ideal, step-like absorptance $a_{step}(E)$, as a function of its band-gap energy E_g and the external LED quantum efficiency Q_{LED}, which is linked by the reciprocity relation with the non-radiative recombination losses. The white line indicates the ideal band gap as a function of Q_{LED} showing that the higher the losses, the larger this ideal band gap and the lower the maximum efficiency of the solar cell that can be achieved. The black lines mark equipotential lines at efficiencies of 20, 25, and 30%

absorption and discuss the implications for the design criteria of organic solar cells from non-fullerene acceptors.

Simulations with ideal collection and absorption properties. In order to illustrate the fundamental impact of non-radiative losses on the efficiency of a solar cell, the first simulations consider a solar cell with ideal collection and absorption properties, characterized by a step-like absorptance

$$a_{step}(E) = \begin{cases} 0, & E < E_g \\ 1, & E \geq E_g \end{cases} \tag{9}$$

Fig. 3 shows the contour plot of the resulting efficiency η as a function of band-gap energy E_g and the amount of non-radiative recombination losses expressed by the external LED quantum efficiency Q_{LED}. The external LED quantum efficiency Q_{LED} varies between 1 and 10^{-8}, which approximately equates to voltage losses in the range from 0 to 480 mV ($\approx$60 mV per decade). First of all, the contour plot shows that the magnitude of non-radiative losses determines the efficiency limit of the solar cell, since these losses reduce the maximum open-circuit voltage. If non-radiative losses do not occur ($Q_{LED} = 1$), the efficiency η reaches the Shockley–Queisser limit[69]. But with increasing losses, the efficiency of the solar cell decreases. Besides, non-radiative losses affect the ideal band-gap energy E_g at which the maximum efficiency is achieved for the respective amount of losses. The white line in Fig. 3 highlights this dependence and illustrates that the ideal band-gap shifts with increasing losses to higher energies. The discrete steps of the ideal band-gap curve are not caused by the discretization of the numerical simulation, but by the spectral profile of the solar spectrum (AM 1.5G), which shows abrupt dips due to molecular absorption (e.g., of O_2, O_3, H_2O, and CO_2) in the atmosphere.

Simulations with parameterized absorption coefficients. In this section, we investigate what the ideal band gaps should be in case
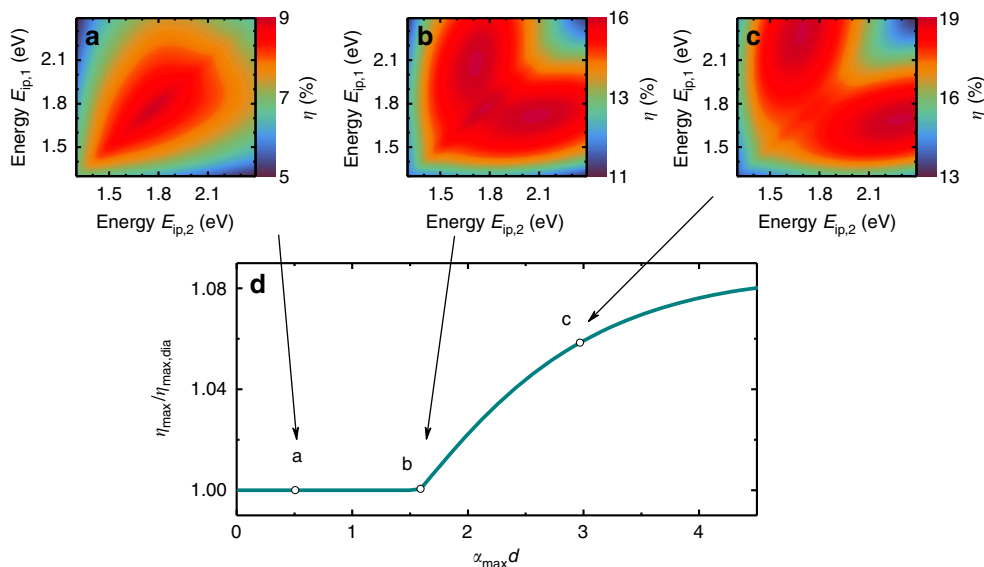

Fig. 4 Simulations of an organic solar cell with parameterized absorption coefficients and ideal collection. (**a–c**) Examples of the simulated efficiency η of an organic solar cell for three different value of the key parameter $\alpha_{max}d$ as a function of the inflection-point energies $E_{ip,1}$ and $E_{ip,2}$ of the absorption coefficients $\alpha_1(E)$ and $\alpha_2(E)$ describing the donor and acceptor material in the blend. For small values of $\alpha_{max}d$ the highest efficiency results for equal energies of $E_{ip,1}$ and $E_{ip,2}$, located on the diagonal of the contour plot, which means that a congruent absorption behavior of donor and acceptor is more efficient in comparison to a complementary one. The opposite applies for large values of $\alpha_{max}d$, as shown in (**c**), since the highest efficiencies occur for off-diagonal, that is, different values of $E_{ip,1}$ and $E_{ip,2}$. (**d**) Ratio of the absolute efficiency maximum η_{max} and the maximum efficiency $\eta_{max,dia}$ on the main diagonal as a function of $\alpha_{max}d$. The course highlights the transition from the absolute maximum efficiency for a congruent arrangement of $\alpha_1(E)$ and $\alpha_2(E)$ toward the maximum for complementary absorption behavior

the active layer consists of a donor–acceptor blend with two molecules that equally contribute to the total absorptance $a_{eff}(E)$. Within the scope of this study, we use the model and the equations introduced in the subsection "Model" to determine the solar cell efficiency η. For this purpose, we shift the two absorption coefficients $\alpha_1(E)$ and $\alpha_2(E)$ representing the donor and acceptor of the blend material by varying their inflection-point energies $E_{ip,1}$ and $E_{ip,2}$ (Fig. 1b). The corresponding simulation parameters are listed in Supplementary Table 1. For each step of the numerical simulation the effective absorption coefficient $\alpha_{eff}(E)$ is formed. For each of these effective absorption coefficients, we subsequently calculate the efficiency η for a set of different layer thicknesses d. As outlined in the subsection "Model," we consider this variation as a function of the key parameter $\alpha_{max}d$. The contour plots in Fig. 4a–c represent the dependence of the efficiency η on the inflection-point energies $E_{ip,1}$ and $E_{ip,2}$ for three different values of $\alpha_{max}d$. The efficiency values on the main diagonals correspond to a congruent configuration of the two absorption coefficients ($E_{ip,1} = E_{ip,2}$). In contrast, the off-diagonal combinations with different inflection-point energies belong to a complementary absorption behavior of donor and acceptor. The comparison of these three contour plots in Fig. 4a–c illustrates that the parameter $\alpha_{max}d$ has a decisive influence on which absorption behavior—congruent or complementary—achieves the highest efficiency for a given $\alpha_{max}d$.

For small values of $\alpha_{max}d$, the maximum is on the main diagonal, implying that a congruent arrangement of the absorption coefficients leads to the highest efficiencies (Fig. 4a). In this case, the choice of two complementary absorbing materials is even less favorable.

The efficiency of the solar cell continuously increases with increasing $\alpha_{max}d$ for all combinations of $E_{ip,1}$ and $E_{ip,2}$, but more strongly for the complementary absorption. Consequently, at a value of $\alpha_{max}d \approx 1.6$, the complementary arrangement of the absorption coefficients finally reaches a higher efficiency (Fig. 4b). From then on, an efficiency gain is achieved by selecting two absorption coefficients $\alpha_1(E)$ and $\alpha_2(E)$ with different inflection-point energies for the active blend. Fig. 4d summarizes these trends and shows the ratio of the absolute maximum efficiency η_{max} and the maximum efficiency $\eta_{max,dia}$ on the main diagonal as a function of $\alpha_{max}d$.

For a better understanding of the dependence of the maximum efficiency on $\alpha_{max}d$, one should take a look at the shape of the solar spectrum ϕ_{sun} (Fig. 5a). Since this spectrum does not

provide a constant photon flux over energy, the short-circuit current density J_{sc}—proportional to the area under the respective curves in Fig. 5a—is strongly affected by the energetic position of the absorptance $a(E)$. Due to the weighting with the solar spectrum, it is even possible to ultimately produce higher short-circuit current densities with a lower overall absorptance. A corresponding example in Fig. 5a, b highlights this fact, where the active layer with a congruent absorptance (Fig. 5b) harvests more photons than the one with the complementary even if its overall absorptance is lower. This example shows that a loss in absorptance at higher photon energies is less relevant because
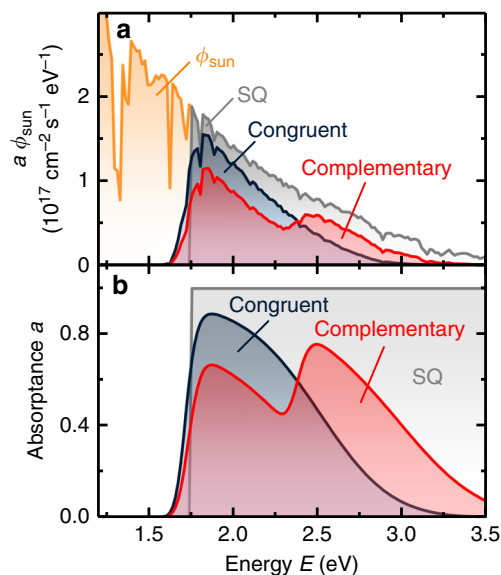

Fig. 5 Comparison between different absorption characteristics. Comparison between (**a**) the product of the AM 1.5G solar spectrum ϕ_{sun} and the absorptance a of a congruent (blue) and a complementary (red) absorbing blend layer. The corresponding absorptance a is shown in (**b**). This example shows that even if the overall absorptance of a congruent arrangement of $\alpha_1(E)$ and $\alpha_2(E)$ is lower, its short-circuit current density may be higher in the end. The corresponding values of the parameters are $E_{ip,1} = 1.75$ eV, $E_{ip,2,con} = 1.75$ eV, $E_{ip,2,comp} = 2.4$ eV, and $d = 68$ nm, the others are the standard values listed in Supplementary Table 1
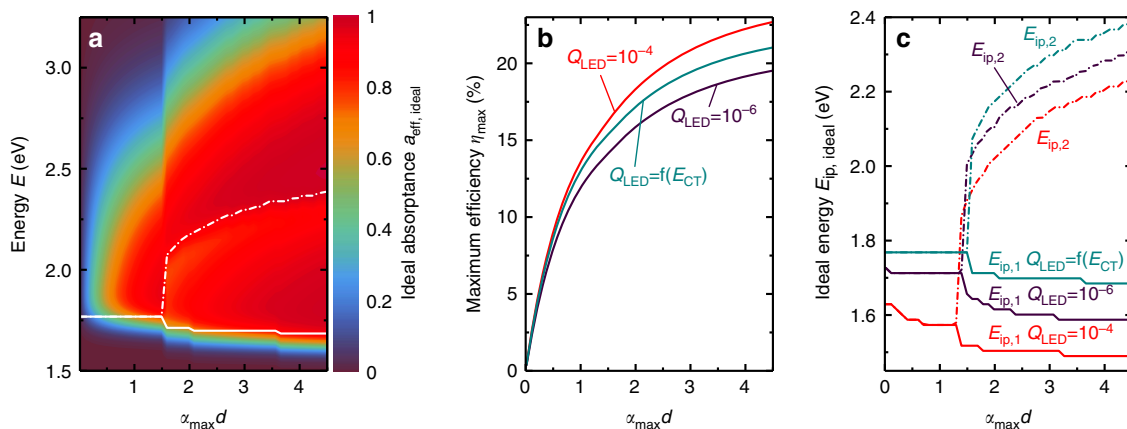

Fig. 6 Beneficial blend parameters resulting from simulations. (**a**) Absorptance $a_{eff,ideal}(E)$ of the blend layer, which leads to the highest efficiency η_{max} at the respective value of $\alpha_{max}d$. The white lines indicate the corresponding inflection-point energies $E_{ip,1}$ and $E_{ip,2}$ of the absorption coefficients of the donor and acceptor. (**b**) The maximum efficiency η_{max}, both for energy-gap-dependent, non-radiative losses (cyan) according to Eqs. (3) and (6) and for constant non-radiative losses (red, purple). (**c**) The corresponding ideal inflection-point energies $E_{ip,ideal}$

of the reduced photon flux in the solar spectrum for energies above 2.5 eV.

Fig. 6a shows the ideal absorptance $a_{eff,ideal}$ of the blend, for which the highest efficiency (Fig. 6b) can be obtained, as a function of $\alpha_{max}d$. For small values of $\alpha_{max}d$, it is more efficient that both organic materials absorb at low energies to exploit the higher photon flux in the low-energy range of the solar spectrum. However, if $\alpha_{max}d$ increases and thus the absorptance in the low-energy region becomes high, it is at some point more beneficial to arrange the absorption coefficients of the donor and the acceptor in a complementary manner to cover a wide energy range. The larger the absorption coefficients of the molecules (larger α_{max}), the smaller the thicknesses needed to reach this transition point. Additionally, in this figure the transition from the maximum efficiency for a congruent arrangement at small values of $\alpha_{max}d$ to one for a complementary arrangement at

large $\alpha_{max}d$ is directly apparent. The white lines mark the corresponding inflection-point energies $E_{ip,1}$ and $E_{ip,2}$, which are shown again in Fig. 6c as cyan lines for the sake of clarity. The additional curves in Fig. 6c of the resulting ideal band gaps, when non-radiative losses were kept constant in the simulations, further emphasize that the general trend also holds for constant values of Q_{LED}. However, the ideal band gaps, i.e., inflection-point energies $E_{ip,1}$ and $E_{ip,2}$ shift with higher non-radiative losses to higher energy.

Simulations with optical interferences and collection losses. So far, the efficiency calculations are based on two simplifications: (i) absorption follows Lambert–Beer and (ii) electronic losses are neglected meaning that all photo-generated charge carriers are extracted and contribute to the current—independent of applied voltage. When the first assumption is dropped by including
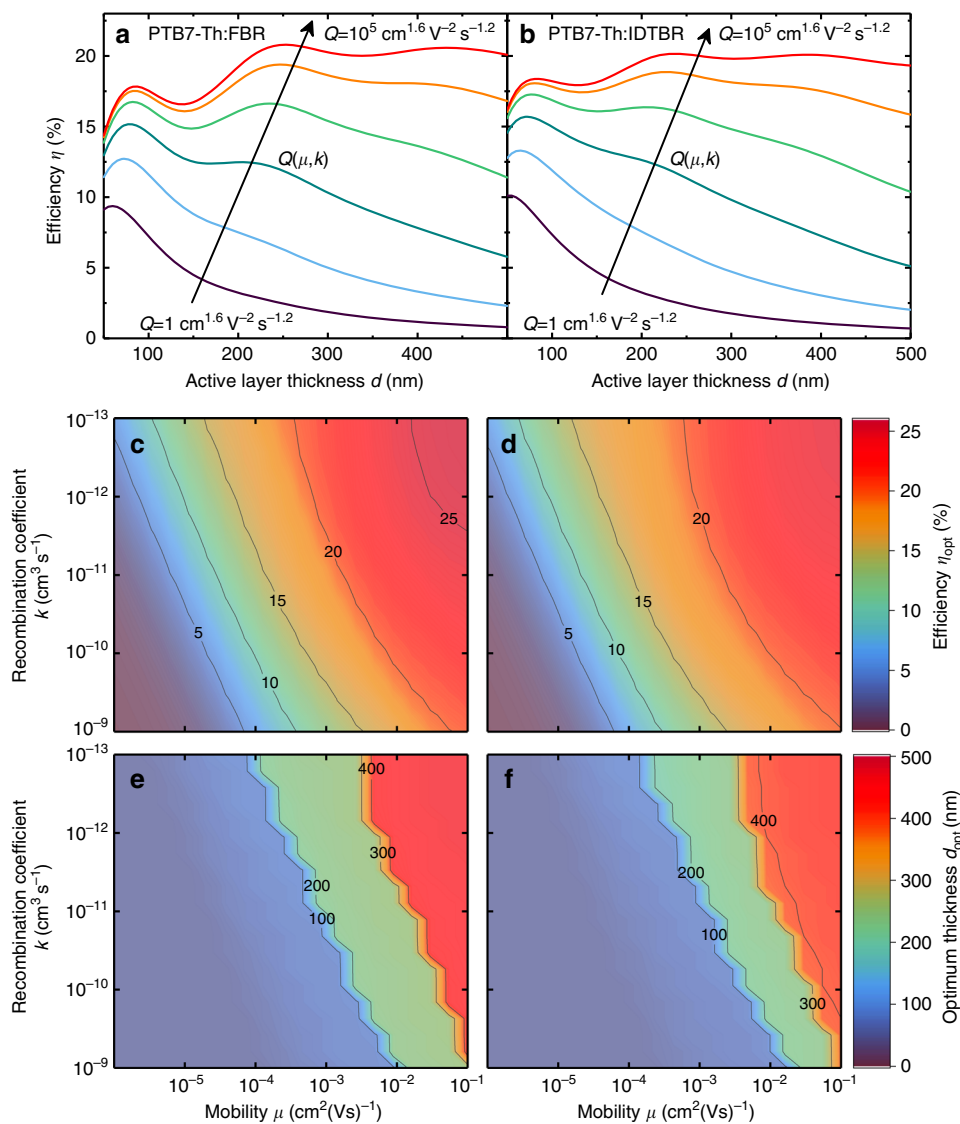

Fig. 7 Simulation with optical interferences and collection losses. Device performance obtained by drift-diffusion simulations based on experimental optical data of a system with (**a**, **c**, **e**) complementary (PTB7-Th:FBR) and (**b**, **d**, **f**) congruent absorption (PTB7-Th:IDTBR). Optical simulations account for interference which leads to efficiency maxima at certain active layer thicknesses in (**a**) and (**b**). Different values of the electronic quality factor Q lead to qualitatively different thickness dependence. High Qs lead to higher gains in maximum efficiency for (**a**) complementary and (**b**) congruent absorption. The general increase in efficiency, evaluated at the optimum thickness, with higher Qs—meaning higher mobility and lower recombination coefficient—is further illustrated in (**c**) and (**d**). The attainable efficiency varies stronger with Q in the (**c**) complementary than in the (**d**) congruent case. For a large range of Qs in (**e**, **f**), the depicted optimum active layer thickness only takes discrete values around the interference maxima visible in (**a**) and (**b**). A transition to a higher optimum thickness requires lower Q values for (**e**) complementary than (**f**) congruent absorption

optical interference in the layer stack, maxima appear in the thickness dependence of absorptance and short-circuit current density (Supplementary Fig. 4a, b). These maxima transfer to the efficiency-thickness relation as can be seen in Fig. 7a, b, which depict the two discussed cases of complementary (PTB7-Th:FBR) and congruent (PTB7-Th:IDTBR) absorption. When the second assumption is dropped by accounting for finite mobilities and recombination coefficients, the *FF* becomes thickness dependent (Supplementary Fig. 4c, d). The different behavior is parametrized by the electronic quality factor Q in Eq. (8), which is varied along the different curves in Fig. 7a, b. Higher Qs generally result in higher efficiencies, which holds for both studied blend systems. The efficiency increase with higher mobilities and lower recombination coefficients—and thus larger Qs—is also depicted in Fig. 7c, d. Figure 7a, b show that for both cases of complementary and congruent absorption, an active layer thickness around the second (or higher) interference maximum leads to an improved efficiency only for a sufficiently large Q. Interference thus discretize the optimum thickness at the first, second, or third absorption maximum. These jumps in optimum thickness are observed clearly in Fig. 7e, f where the optimum thickness is plotted for a large range of mobilities and recombination coefficients.

While complementary and congruent absorption behave qualitatively similar in many aspects, there are certain notable differences between the two cases. Most importantly, the increase in efficiency from the first to the second maximum—enabled by sufficiently large Qs—is less for the congruent case of IDTBR as can be seen by comparing Fig. 7a, b. The closer spacing of lines with equal efficiency in the case of complementary absorption in Fig. 7c compared to congruent absorption in Fig. 7d express the same effect. The thickness dependence of the efficiency is determined by the gain in absorptance and J_{sc} versus the loss in *FF* with increasing thickness. For congruent absorption large part of the incident light is already absorbed in a thin active layer and the achievable gain in absorptance for a thicker layer is low compared to the case of complementary absorption. In the latter case, the absorptance is low over a larger spectral range for a thin device and by increasing the thickness, the absolute value of absorptance increases significantly. Since the drop in *FF* with thickness and electronic quality is the same for both systems, the attainable gain in absorptance decides if a thicker layer is favorable in terms of device efficiency. For the same reasons not only the attainable gain in efficiency differs between a complementary and a congruent absorbing system but also the value of Q that is necessary to reach an efficiency improvement. For the simulations shown in Fig. 7a, b, a jump to the second interference maximum requires $Q \gtrsim 10^3$ cm$^{1.6}$ V^{-2} s$^{-1.2}$ for the complementary absorbing PTB7-Th:FBR, while the congruent absorbing PTB7-Th:IDTBR requires $Q \gtrsim 10^4$ cm$^{1.6}$ V^{-2} s$^{-1.2}$. Also, for PTB7-Th:IDTBR in Fig. 7f the transition to larger optimum thicknesses is shifted to higher values of k and μ, implying a higher Q, compared to PTB7-Th:FBR in Fig. 7e. Thus, for a blend with complementary absorption the threshold for Q, above which thicker active layers are more efficient, is generally lower.

Discussion

Donor and non-fullerene acceptor molecules absorb only well in a limited spectral energy region of about ~0.5 eV. By combining different donor and non-fullerene acceptor molecules, which contribute roughly equal amounts to the total absorptance, different absorption characteristics of the blend material can be realized, ranging from congruent ($E_{ip,1} = E_{ip,2}$) to complementary ($E_{ip,2} \gg E_{ip,1}$). For which of these different combinations the highest efficiency is obtainable depends to a large extent on how the incident photon flux ϕ_{sun} provided by the sun is exploited. This photon flux per electron volt of the solar spectrum is much higher in the low-energy range and decreases with increasing energy. Thus, the energetic position of the total absorption $a(E)$ strongly influences the maximum achievable short-circuit current density and finally the solar cell efficiency η.

We have shown that for small layer thicknesses, it is more beneficial to arrange the absorption coefficients of the donor and the acceptor in a congruent manner in order to make the best possible use of the high photon flux ϕ_{sun} in the low-energy range. Covering a broad energy range by combining two molecules that absorb complementarily is only more efficient if the absorptance of the active layer in the low-energy range is still high which requires molecules that absorb very strongly or active layers with thicknesses around the second interference maximum or higher. Such thick layers are only feasible if charge-carrier collection at the maximum power point is sufficiently efficient.

References

1. Vezie, M. S. et al. Exploring the origin of high optical absorption in conjugated polymers. *Nat. Mater.* **15**, 746 (2016).
2. Bakulin, A. A. et al. The role of driving energy and delocalized states for charge separation in organic semiconductors. *Science* **335**, 1340–1344 (2012).
3. Gélinas, S. et al. Ultrafast long-range charge separation in organic semiconductor photovoltaic diodes. *Science* **343**, 512–516 (2014).
4. Clarke, T. M. & Durrant, J. R. Charge photogeneration in organic solar cells. *Chem. Rev.* **110**, 6736–6767 (2010).
5. Jakowetz, A. C. et al. What controls the rate of ultrafast charge transfer and charge separation efficiency in organic photovoltaic blends. *J. Am. Chem. Soc.* **138**, 11672–11679 (2016).
6. Jamieson, F. C. et al. Fullerene crystallisation as a key driver of charge separation in polymer/fullerene bulk heterojunction solar cells. *Chem. Sci.* **3**, 485–492 (2012).
7. Dimitrov, S. D. et al. Efficient charge photogeneration by the dissociation of PC70BM excitons in polymer/fullerene solar cells. *J. Phys. Chem. Lett.* **3**, 140–144 (2011).
8. Lee, J. et al. Charge transfer state versus hot exciton dissociation in polymer−fullerene blended solar cells. *J. Am. Chem. Soc.* **132**, 11878–11880 (2010).
9. Foster, S. et al. Electron collection as a limit to polymer:PCBM solar cell efficiency: effect of blend microstructure on carrier mobility and device performance in PTB7:PCBM. *Adv. Energy Mater.* **4**, 1400311 (2014).
10. Park, S. H. et al. Bulk heterojunction solar cells with internal quantum efficiency approaching 100%. *Nat. Photonics* **3**, 297–302 (2009).
11. Zhang, X. et al. A potential perylene diimide dimer-based acceptor material for highly efficient solution-processed non-fullerene organic solar cells with 4.03% efficiency. *Adv. Mater.* **25**, 5791–5797 (2013).
12. Schwenn, P. E. et al. A small molecule non-fullerene electron acceptor for organic solar cells. *Adv. Energy Mater.* **1**, 73–81 (2011).
13. Zheng, Z. et al. Efficient charge transfer and fine-tuned energy level alignment in a THF-processed fullerene-free organic solar cell with 11.3% efficiency. *Adv. Mater.* **29**, 1604241 (2017).
14. Li, S. et al. Energy-level modulation of small-molecule electron acceptors to achieve over 12% efficiency in polymer solar cells. *Adv. Mater.* **28**, 9423–9429 (2016).

15. Baran, D. et al. Reducing the efficiency-stability-cost gap of organic photovoltaics with highly efficient and stable small molecule acceptor ternary solar cells. *Nat. Mater.* **16**, 363–369 (2017).

16. Zhao, W. et al. Fullerene-free polymer solar cells with over 11% efficiency and excellent thermal stability. *Adv. Mater.* **28**, 4734–4739 (2016).

17. Zhang, J. et al. Conjugated polymer–small molecule alloy leads to high efficient ternary organic solar cells. *J. Am. Chem. Soc.* **137**, 8176–8183 (2015).

18. Baran, D. et al. Reduced voltage losses yield 10% efficient fullerene free organic solar cells with 1 V open circuit voltages. *Energy Environ. Sci.* **9**, 3783–3793 (2016).

19. Zhao, W. et al. Molecular optimization enables over 13% efficiency in organic solar cells. *J. Am. Chem. Soc.* **139**, 7148–7151 (2017).

20. Yao, H. et al. Design, synthesis, and photovoltaic characterization of a small molecular acceptor with an ultra-narrow band gap. *Angew. Chem. Int. Ed.* **56**, 3045–3049 (2017).

21. Hou, J., Inganäs, O., Friend, R. H. & Gao, F. Organic solar cells based on non-fullerene acceptors. *Nat. Mater.* **17**, 119 (2018).

22. Mishra, A. et al. Unprecedented low energy losses in organic solar cells with high external quantum efficiencies by employing non-fullerene electron acceptors. *J. Mater. Chem. A* **5**, 14887–14897 (2017).

23. Li, Y. et al. Non-fullerene acceptor with low energy loss and high external quantum efficiency: towards high performance polymer solar cells. *J. Mater. Chem. A* **4**, 5890–5897 (2016).

24. Nikolis, V. C. et al. Reducing voltage losses in cascade organic solar cells while maintaining high external quantum efficiencies. *Adv. Energy Mater.* **7**, 1700855 (2017).

25. Faist, M. A. et al. Understanding the reduced efficiencies of organic solar cells employing fullerene multiadducts as acceptors. *Adv. Energy Mater.* **3**, 744–752 (2013).

26. Felekidis, N., Wang, E. & Kemerink, M. Open circuit voltage and efficiency in ternary organic photovoltaic blends. *Energy Environ. Sci.* **9**, 257–266 (2016).

27. Holliday, S. et al. A rhodanine flanked nonfullerene acceptor for solution-processed organic photovoltaics. *J. Am. Chem. Soc.* **137**, 898–904 (2015).

28. Holliday, S. et al. High-efficiency and air-stable P3HT-based polymer solar cells with a new non-fullerene acceptor. *Nat. Commun.* **7**, 11585 (2016).

29. Chen, J. D. et al. Single-junction polymer solar cells exceeding 10% power conversion efficiency. *Adv. Mater.* **27**, 1035–1041 (2015).

30. Etxebarria, I., Ajuria, J. & Pacios, R. Solution-processable polymeric solar cells: a review on materials, strategies and cell architectures to overcome 10%. *Org. Electron.* **19**, 34–60 (2015).

31. Blank, B., Kirchartz, T., Lany, S. & Rau, U. Selection metric for photovoltaic materials screening based on detailed-balance analysis. *Phys. Rev. Appl.* **8**, 024032 (2017).

32. Janssen, R. A. J. & Nelson, J. Factors limiting device efficiency in organic photovoltaics. *Adv. Mater.* **25**, 1847–1858 (2013).

33. Koster, L. J. A., Shaheen, S. E., & Hummelen, J. C. Pathways to a new efficiency regime for organic solar cells. *Adv. Energy Mater.* **2**, 1246–1253 (2012).

34. Liu, J. et al. Fast charge separation in a non-fullerene organic solar cell with a small driving force. *Nat. Energy* **1**, 16089 (2016).

35. Wagenpfahl, A.J. *Numerical Simulations on Limitations and Optimization Strategies of Organic Solar Cells.* PhD thesis, University of Würzburg (2013).

36. Credgington, D. & Durrant, J. R. Insights from transient optoelectronic analyses on the open-circuit voltage of organic solar cells. *J. Phys. Chem. Lett.* **3**, 1465–1478 (2012).

37. Burke, T. M., Sweetnam, S., Vandewal, K. & McGehee, M. D. Beyond Langevin recombination: how equilibrium between free carriers and charge transfer states determines the open-circuit voltage of organic solar cells. *Adv. Energy Mater.* **5**, 1500123 (2015).

38. Hawks, S. A. et al. Relating recombination, density of states, and device performance in an efficient polymer:fullerene organic solar cell blend. *Adv. Energy Mater.* **3**, 1201–1209 (2013).

39. Benduhn, J. et al. Intrinsic non-radiative voltage losses in fullerene-based organic solar cells. *Nat. Energy* **2**, 17053 (2017).

40. Lang, D., Grimmeiss, H., Meijer, E. & Jaros, M. Complex nature of gold-related deep levels in silicon. *Phys. Rev. B* **22**, 3917 (1980).

41. Lang, D. & Henry, C. Nonradiative recombination at deep levels in GaAs and GaP by lattice-relaxation multiphonon emission. *Phys. Rev. Lett.* **35**, 1525 (1975).

42. Englman, R. & Jortner, J. The energy gap law for radiationless transitions in large molecules. *Mol. Phys.* **18**, 145–164 (1970).

43. Gould, I. R. et al. Radiative and nonradiative electron transfer in contact radical-ion pairs. *Chem. Phys.* **176**, 439–456 (1993).

44. Chen, X. K., Ravva, M. K., Li, H., Ryno, S. M. & Brédas, J. L. Effect of molecular packing and charge delocalization on the nonradiative recombination of charge-transfer states in organic solar cells. *Adv. Energy Mater.* **6**, 1601325 (2016).

45. Chen, X. K. & Brédas, J. L. Voltage losses in organic solar cells: understanding the contributions of intramolecular vibrations to nonradiative recombinations. *Adv. Energy Mater.* **8**, 1702227 (2017).

46. Ridley, B. K. On the multiphonon capture rate in semiconductors. *Solid Electron.* **21**, 1319–1323 (1978).

47. Ridley, B. K. *Quantum Processes in Semiconductors* 5th edn, 220–227 (Oxford Univ. Press, Oxford, 2013).

48. Schenk, A. An improved approach to the Shockley–Read–Hall recombination in inhomogeneous fields of space-charge regions. *J. Appl. Phys.* **71**, 3339–3349 (1992).

49. Bozyigit, D. et al. Soft surfaces of nanomaterials enable strong phonon interactions. *Nature* **531**, 618–623 (2016).

50. Vandewal, K., Tvingstedt, K., Gadisa, A., Inganäs, O. & Manca, J. V. Relating the open-circuit voltage to interface molecular properties of donor:acceptor bulk heterojunction solar cells. *Phys. Rev. B* **81**, 125204 (2010).

51. Smestad, G. & Ries, H. Luminescence and current–voltage characteristics of solar cells and optoelectronic devices. *Sol. Energy Mater. Sol. Cells* **25**, 51–71 (1992).

52. Rau, U. Reciprocity relation between photovoltaic quantum efficiency and electroluminescent emission of solar cells. *Phys. Rev. B* **76**, 085303 (2007).

53. Rau, U., Blank, B., Müller, T. C. M. & Kirchartz, T. Efficiency potential of photovoltaic materials and devices unveiled by detailed-balance analysis. *Phys. Rev. Appl.* **7**, 044016 (2017).

54. Green, M. A. Solar cell fill factors: general graph and empirical expressions. *Solid Electron.* **24**, 788–789 (1981).

55. Kaienburg, P., Rau, U. & Kirchartz, T. Extracting information about the electronic quality of organic solar-cell absorbers from fill factor and thickness. *Phys. Rev. Appl.* **6**, 024001 (2016).

56. Kirchartz, T., Agostinelli, T., Campoy-Quiles, M., Gong, W. & Nelson, J. Understanding the thickness-dependent performance of organic bulk heterojunction solar cells: the influence of mobility, lifetime, and space charge. *J. Phys. Chem. Lett.* **3**, 3470–3475 (2012).

57. Bartesaghi, D. et al. Competition between recombination and extraction of free charges determines the fill factor of organic solar cells. *Nat. Commun.* **6**, 7083 (2015).

58. Crandall, R. S. Transport in hydrogenated amorphous silicon p–i–n solar cells. *J. Appl. Phys.* **53**, 3350–3352 (1982).

59. Crandall, R. S. Modeling of thin film solar cells: uniform field approximation. *J. Appl. Phys.* **54**, 7176–7186 (1983).

60. Guo, B. et al. High efficiency nonfullerene polymer solar cells with thick active layer and large area. *Adv. Mater.* **29**, 1702291 (2017).

61. Yao, H. et al. Achieving highly efficient nonfullerene organic solar cells with improved intermolecular interaction and open-circuit voltage. *Adv. Mater.* **29**, 1700254 (2017).

62. Ye, L. et al. High-efficiency nonfullerene organic solar cells: critical factors that affect complex multi-length scale morphology and device performance. *Adv. Energy Mater.* **7**, 1602000 (2017).

63. Bin, H. et al. 11.4% Efficiency non-fullerene polymer solar cells with trialkylsilyl substituted 2D-conjugated polymer as donor. *Nat. Commun.* **7**, 13651 (2016).

64. Vohra, V. et al. Efficient inverted polymer solar cells employing favourable molecular orientation. *Nat. Photonics* **9**, 403 (2015).

65. Nguyen, T. L. et al. Semi-crystalline photovoltaic polymers with efficiency exceeding 9% in a ~300 nm thick conventional single-cell device. *Energy Environ. Sci.* **7**, 3040–3051 (2014).

66. Guo, X. et al. Polymer solar cells with enhanced fill factors. *Nat. Photonics* **7**, 825–833 (2013).

67. Liu, Y. et al. Aggregation and morphology control enables multiple cases of high-efficiency polymer solar cells. *Nat. Commun.* **5**, 5293 (2014).

68. Burkhard, G. F., Hoke, E. T. & McGehee, M. D. Accounting for interference, scattering, and electrode absorption to make accurate internal quantum efficiency measurements in organic and other thin solar cells. *Adv. Mater.* **22**, 3293–3297 (2010).

69. Shockley, W. & Queisser, H. J. Detailed balance limit of efficiency of p–n junction solar cells. *J. Appl. Phys.* **32**, 510–519 (1961).

Acknowledgements

Author contributions

L.K., P.K., and T.K. prepared the manuscript. L.K. and P.K. made the simulations. L.K. fabricated solar cell devices and thin films supervised by I.Z. J.F. performed the EL measurements. K.B. and L.K. carried out and analyzed the UV–Vis absorption

measurements and ellipsometry measurements. T.K., I.Z., and B.K. supervised L.K. All authors discussed the results and commented on the manuscript.

Additional information

Competing interests: The authors declare no competing interests.

Reprints and permission information is available online at http://npg.nature.com/reprintsandpermissions/

Publisher's note: Springer Nature remains neutral with regard to jurisdictional claims in published maps and institutional affiliations.